Electronic Supplementary Information

Copper molybdenum sulfide anchored nickel foam: A high performance, binder-free, negative electrode for supercapacitor

Surjit Sahoo[a, #], Karthikeyan Krishnamoorthy[a, #], Parthiban Pazhamalai[a], Sang -Jae Kim[a,b,*]

[a] Nanomaterials and System Lab, Department of Mechatronics Engineering,

Jeju National University, Jeju 63243, South Korea.

[b] Department of Advanced Convergence Science & Technology,

Jeju National University, Jeju 63243, South Korea.

[#]These authors contributed equally.

*Corresponding author. Email: kimsangj@jejunu.ac.kr

1. Experimental section

1.1 Materials

Sodium molybdate ($Na_2MoO_4.2H_2O$), hydrazine monohydrate ($N_2H_4.H_2O$), thioacetamide (CH_3CSNH_2), copper (II) sulfate pentahydrate ($CuSO_4.5H_2O$), ethylene glycol, and sodium sulfate (Na_2SO_4) were purchased from Daejung Chemicals Ltd., South Korea. Nickel Foam (110 PPI, Thickness: 1.0 mm) obtained from HEZE JIAOTONG GROUP (China) were used as the substrate for direct to grow CMS nanostructure. All used Ni foam substrates were thoroughly cleaned with absolute ethanol and DI water many times by ultra-sonication. Then they were dried in an electric oven at 60 °C temperature for 3 h. Afterwards used as the substrate for hydrothermal growth of CMS nanostructure.

1.2 Hydrothermal growth of CMS anchored on Ni foam

A one-pot hydrothermal method was used for the preparation of CMS nanostructure on Ni foam. In a typical synthesis, 60 mg of $Na_2MoO_4.2H_2O$ and 120 mg of CH_3CSNH_2 was dissolved in 60 mL of ethylene glycol by ultra-sonication for one hour. Then 40 mg of Cu_2O was added slowly to the above precursor solution (synthesized using the process given in literature [1]) and kept it for ultra-sonication for two h to form a dark brown solution. After that, the precursor solution was transferred to a 100 mL Teflon lined stainless steel autoclave. The cleaned piece of Ni foam was immersed in the dark brown solution and kept at 150 °C for 15 h. After completion of the hydrothermal reaction, the autoclave was allowed to cool to room temperature naturally and collected the obtained precursor grown on Ni foam. Ni foam was cleaned by ultrasonication approach using repeated rinses of water and absolute ethanol. Finally, the collected Ni foam was dried at 60 °C for 4 h.

1.3 Instrumentation

The as-grown CMS nanostructure on Ni foam were used for different physical characterizations to confirm the structural and morphological analysis. The morphologies of

the as prepared binder free CMS nanostructure on Ni foam was analysed using field-emission scanning electron microscopy (TESCAN, MIRA3) under different magnifications. The chemical elements and its states were analyzed using X-ray photoelectron spectroscopy (XPS) techniques (ESCA-2000, VG Microtech Ltd, Al Kα (1486.6 eV) and binding energies (B.E.) were evaluated using C 1 s (B.E.=284.6 eV) as the reference. The XRD analysis were analysed using X-Ray Diffractometer System (X'pert pro MPD) with Cu-Kα radiation (λ=1.5418 Å) (KBSI, Busan Center). The UV-vis spectroscopy analysis was performed using Optical Spectrometer (UV/VIS/NIR spectrophotometer) Cary 5G, KBSI, Daegu centre). The specific surface area for the CMS/Ni and CMS powder were analysed using Particle and Pore Size Analysis System (UPA-150, ASAP2010, Autopore IV, KBSI, Jeonju Center)

1.4 Electrochemical analysis

The electrochemical performance of as synthesized binder free CMS nanostructure anchored on Ni foam was investigated through cyclic voltammetry (CV), galvanostatic charge–discharge (CD), and electrochemical impedance spectroscopy (EIS) in three electrode system and symmetric device using an AUTOLAB PGSTAT302N electrochemical workstation in 1 M aqueous solution of sodium sulfate (Na_2SO_4) as the electrolyte. For three electrode system freshly prepared a piece of CMS anchored on Ni foam (1×1 cm^2) was used as working electrode, platinum as the counter electrode, and Ag/AgCl as the reference electrode. The electroactive mass of the CMS anchored on Ni foam current collector is measured as 1 mg which was calculated from the difference between the mass of the substrate before and after growing of the CMS using Dual-range Semi-micro Balance (AUW-220D, SHIMADZU) with an approximation of five-decimal points.

The binder-free CMS anchored on Ni foam SSC device was fabricated by sandwiching polypropylene separator between two CMS anchored on Ni foam. An aqueous solution of 1 M Na_2SO_4 is used as the electrolyte. The electrochemical performance of SSC

device was investigated through cyclic voltammetry (CV), galvanostatic charge-discharge (CD), and electrochemical impedance spectroscopy (EIS) using an AUTOLAB PGSTAT302N electrochemical workstation.

Electrochemical parameter: The evaluation of specific capacitance (*Csp*) of CMS/Ni electrode was obtained from cyclic voltammetry (CV) and galvanostatic charge-discharge (CD) is given by following relations:[2]

$$Csp = [(\int I\,dV) / (s \times \Delta V \times m)] \ldots\ldots\ldots\ldots\ldots\ldots\ldots\ldots\ldots \quad (1)$$

$$Csp = [(I \times \Delta t) / (\Delta V \times m)] \ldots\ldots\ldots\ldots\ldots\ldots\ldots\ldots \quad (2)$$

The specific capacity (*Qs*) of CMS/Ni electrode was obtained from CV and CD profile using the following relations:[3]

$$Qs = [(\int I\,dV) / (s \times m)] \ldots\ldots\ldots\ldots\ldots\ldots\ldots\ldots \quad (3)$$

$$Qs = (I \times \Delta t) / (m \times 3.6) \ldots\ldots\ldots\ldots\ldots\ldots\ldots\ldots (4)$$

Here, "*Csp*" is the specific capacitance (F g^{-1}), specific capacity "*Qs*" in (mAh g^{-1}), "*I*" is the current (A), "ΔV" is the potential window, "*s*" is the scan rate (mV s^{-1}), "Δt" is the discharge time (s), and "*m*" is the mass of the active material (mg).

The energy density (*E*) and power density (*P*) of the CMS/Ni SSC device were calculated using the following relations:[4]

$$E = (I \times \Delta t \times \Delta V) / (7.2 \times m) \ldots\ldots\ldots\ldots\ldots\ldots\ldots\ldots \quad (5)$$

$$P = (3.6 \times E) / \Delta t \ldots\ldots\ldots\ldots\ldots\ldots\ldots\ldots \quad (6)$$

Here, "*E*" is the energy density (Wh kg^{-1}), "*P*" is the power density (W kg^{-1}), "*I*" is the current (A), "ΔV" is the potential window, "Δt" is the discharge time (s), and "*m*" is the mass of the active material (mg).

The variation of specific capacitance of CMS/Ni electrode with respect to frequency was obtained from the EIS analysis using the relation:[5]

$$Cs = -1/2\pi fz'' \ldots\ldots\ldots\ldots\ldots\ldots\ldots\ldots \quad (7)$$

Here "*Cs*" is the specific capacitance of the device, and "*f*" is the applied frequency, and "*z''*" is the imaginary plot of impedance.

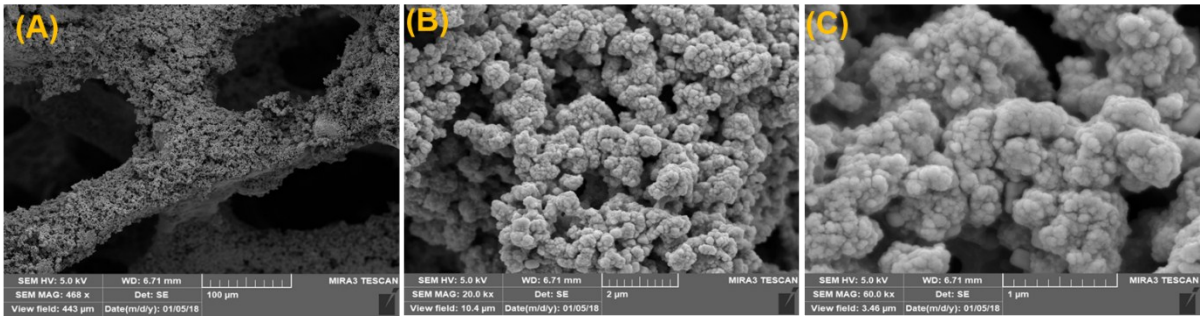

Figure S1. FE-SEM image of CMS anchored on Ni foam.

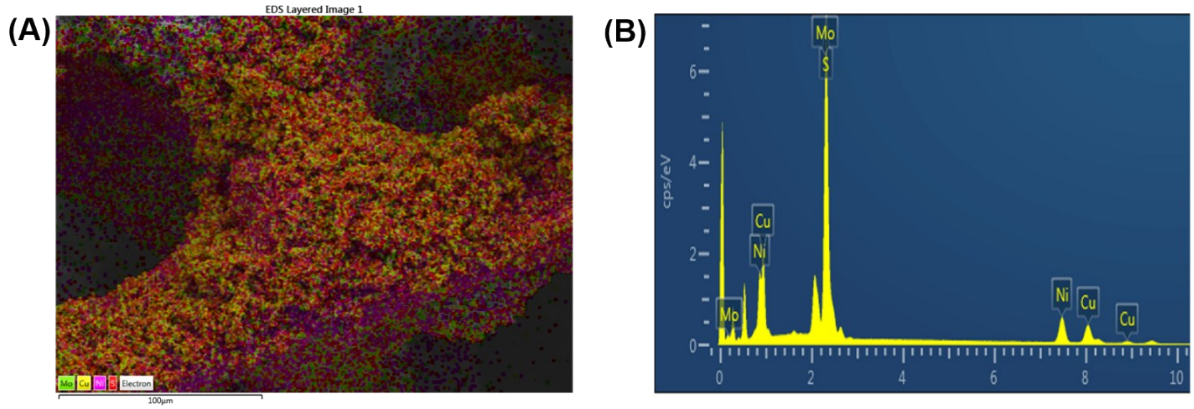

Figure S2. (A) FE-SEM micrographs for elemental mapping and (B) EDS spectrum for CMS anchored on Ni foam.

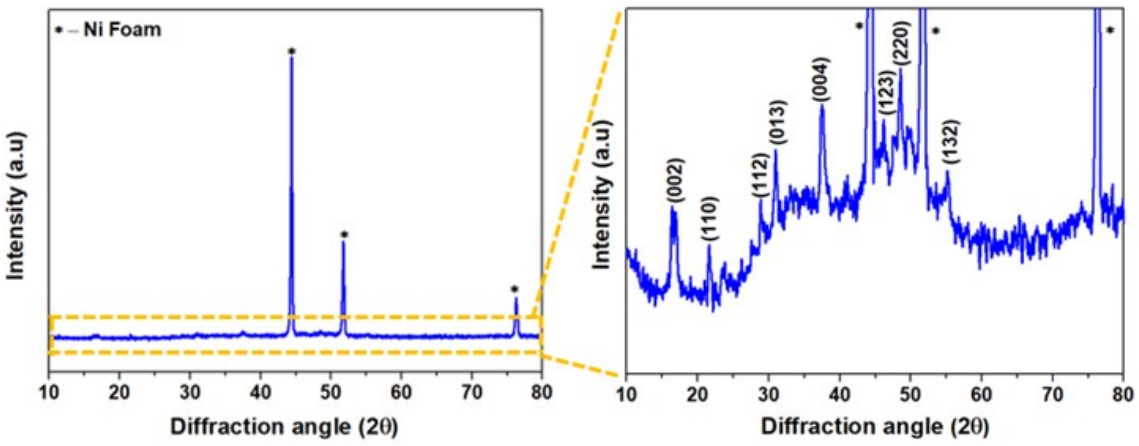

Figure S3. XRD pattern of CMS grown on Ni foam, peaks denoted to (*) correspond to Ni foam.

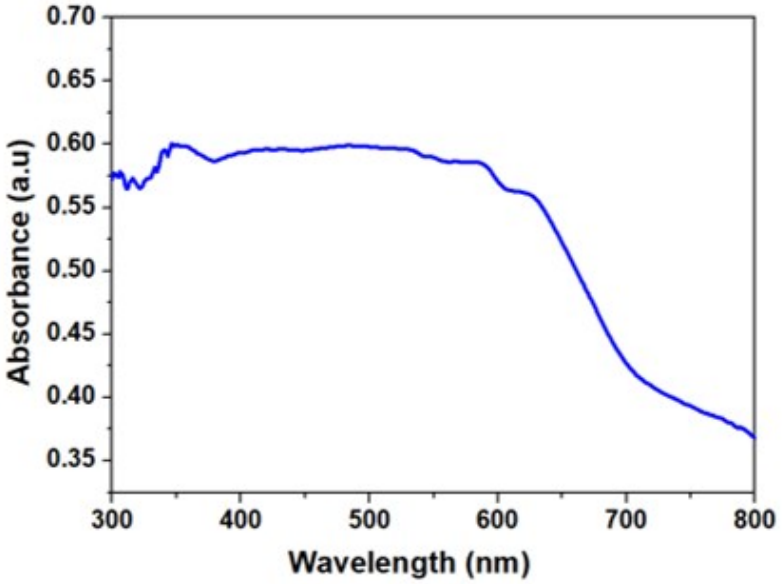

Figure S4. (A) UV–vis absorption spectrum for the CMS nanostructures.

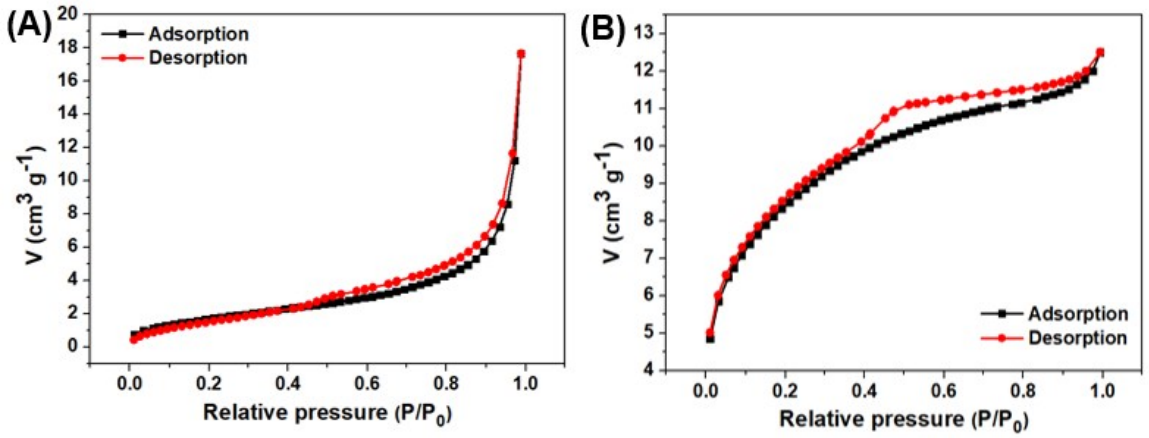

Figure S5. (A) Nitrogen adsorption-desorption isotherm for CMS powder and (B) CMS/Ni foam.

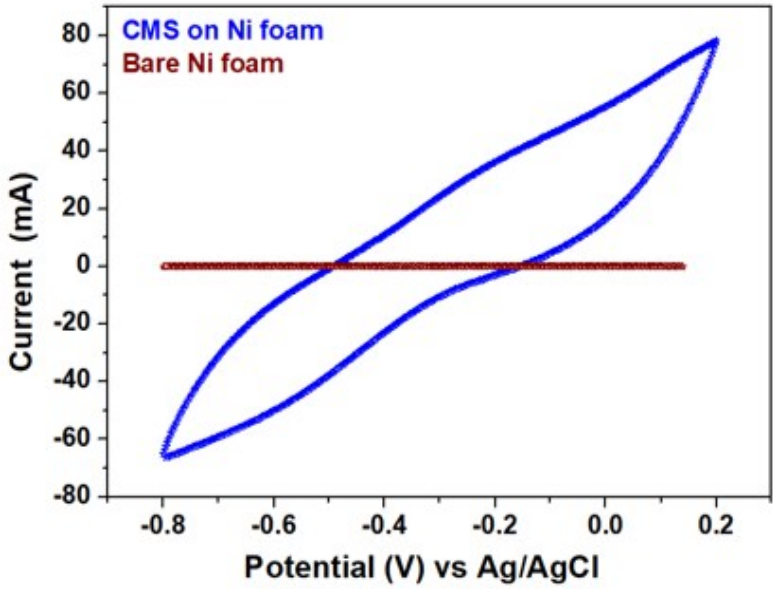

Figure S6. Cyclic voltammetry analysis of bare Ni foam and CMS/Ni electrode in three electrode configuration.

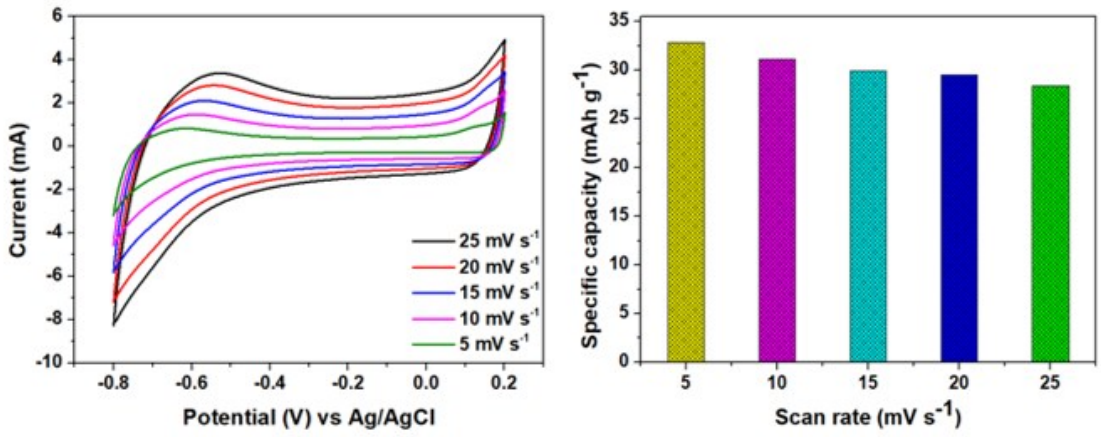

Figure S7. Electrochemical performance of binder-based CMS electrode in three electrode configuration. The three-electrode configuration test of binder-based CMS electrode was performed according to the method reported in our earlier literature.[5]

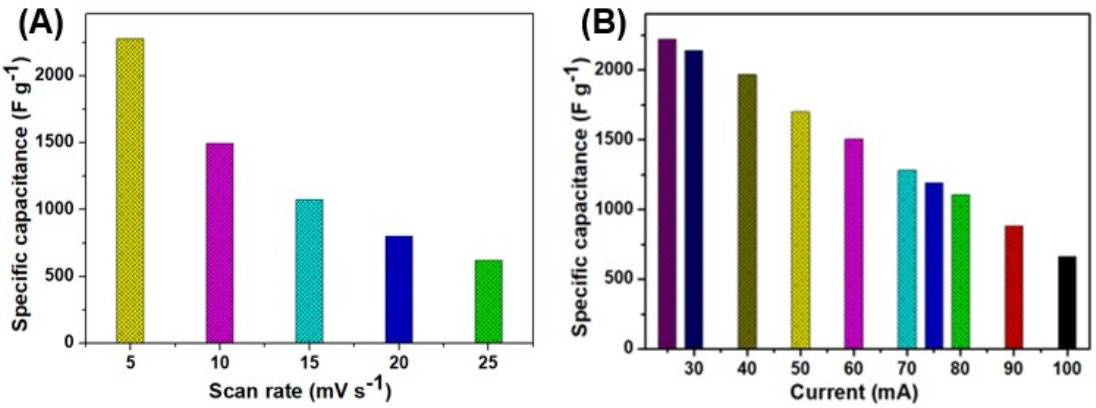

Figure S8. (A) Effect of specific capacitance of CMS/Ni electrode with respect to scan rate, and (B) Effect of specific capacitance of CMS/Ni electrode with respect to current.

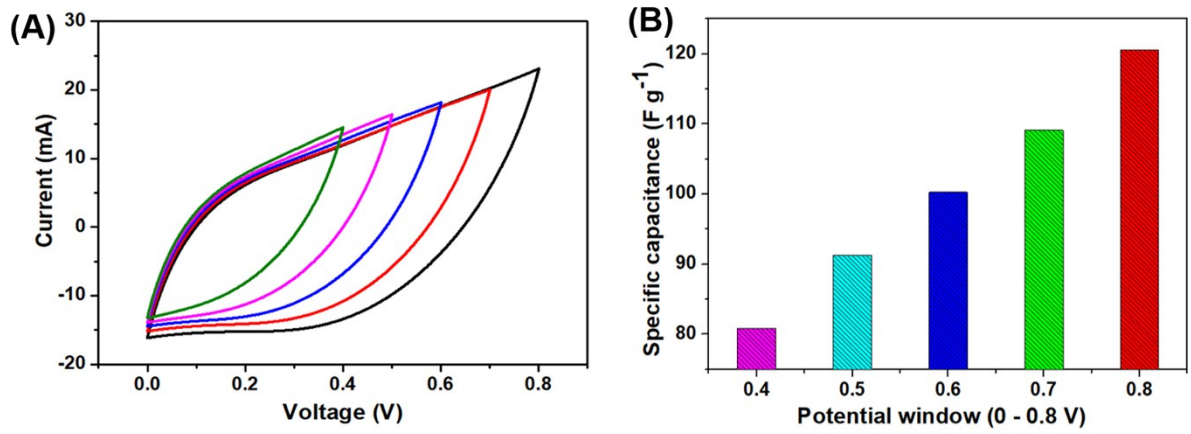

Figure S9. Potential window optimization of CMS/Ni SSC device using cyclic voltammetry: (A) cyclic voltammetric profile at different potential window, and (B) effect of specific capacitance of CMS/Ni SSC device with respect to different operating potential window (OPW).

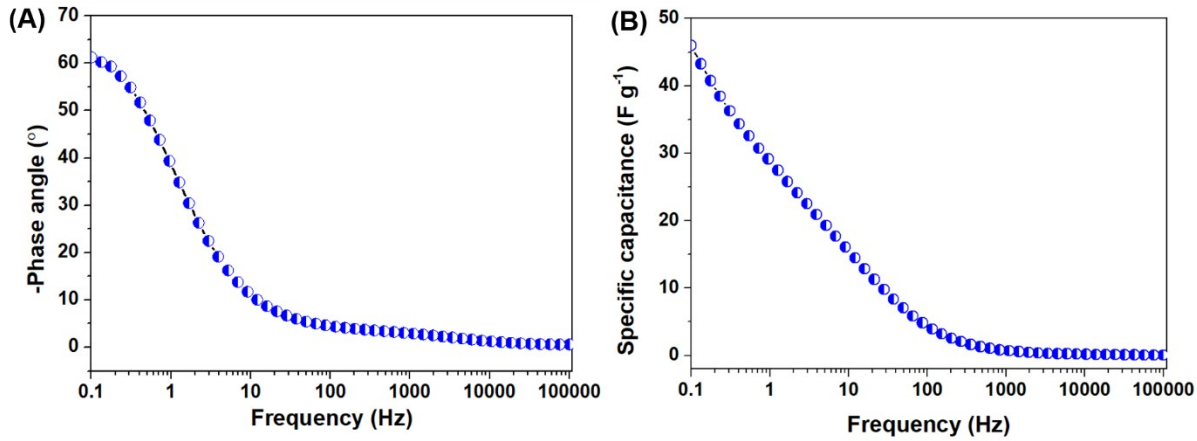

Figure S10. EIS analysis of CMS/Ni SSC device (A) Bode phase angle plot, and (B) Plot of variation of specific capacitance of CMS/Ni SSC device with respect to frequency.

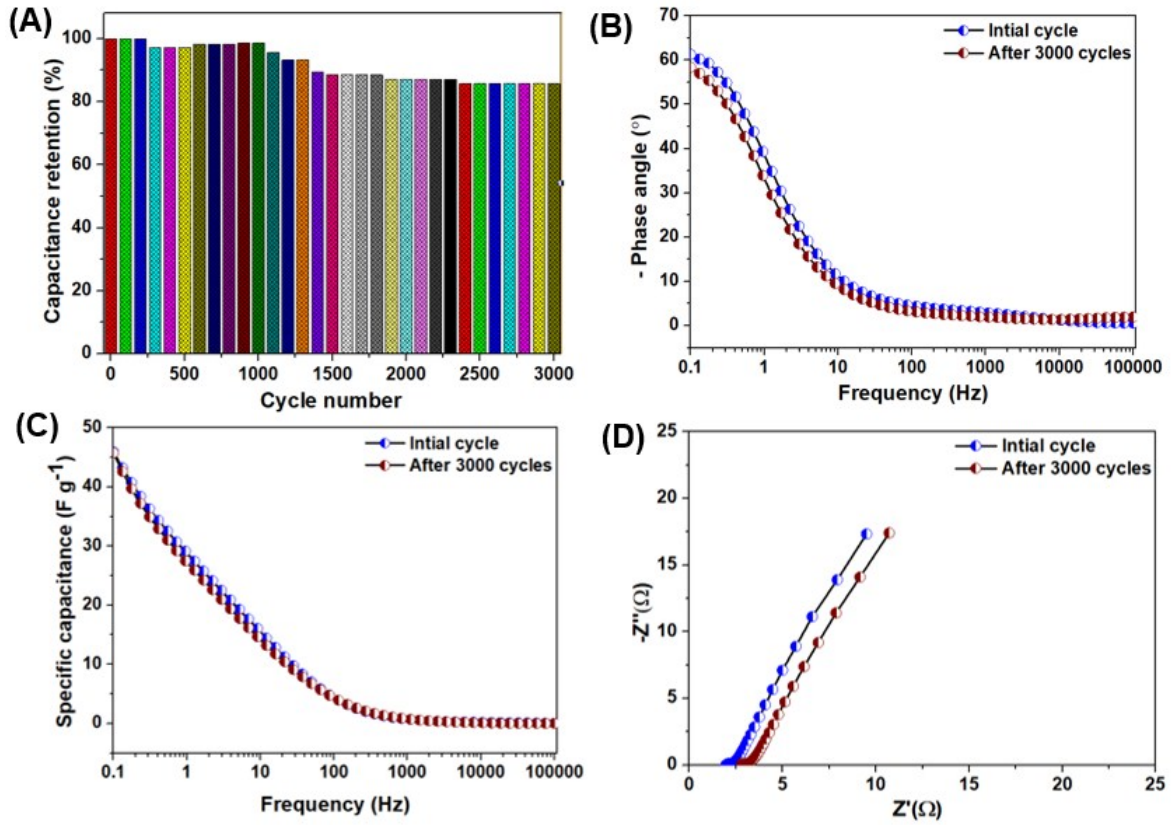

Figure S11. (A) Cyclic stability performance for CMS/Ni SSC device, (B) Bode phase angle plot initial and after 3000 cycles for CMS/Ni SSC device, (C) Plot of variation of specific capacitance of CMS/Ni SSC device with respect to frequency initial and after 3000 cycles for CMS/Ni SSC device, and (D) Nyquist plot of CMS/Ni SSC device measured during initial and after 3000 cycles.

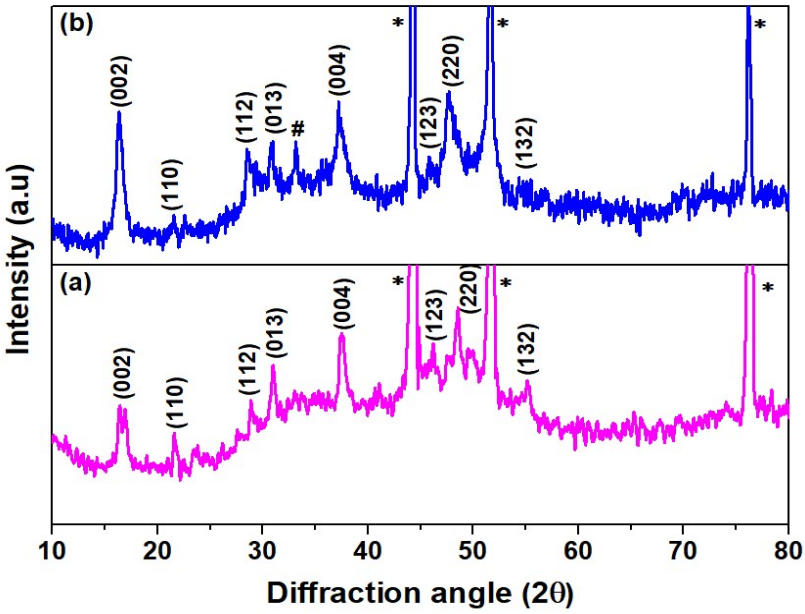

Figure S12. Comparison of XRD spectra for CMS/Ni foam (a) initial and (b) after the cyclic test. The peaks denoted to (*) correspond to Ni foam and (#) to Na_2SO_4.

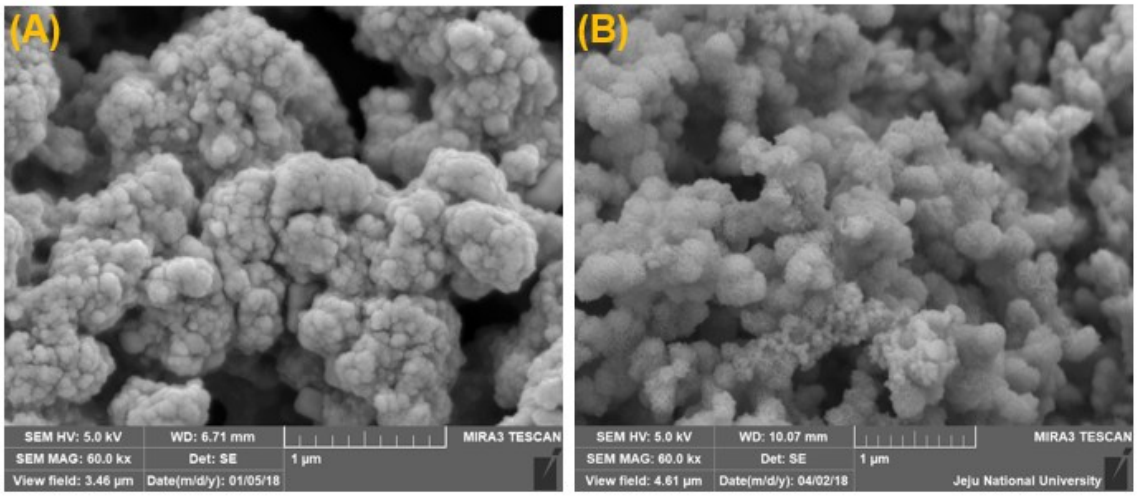

Figure S13. FE-SEM micrograph for CMS/Ni SSC (A) before and (B) after cyclic stability performance.

Table S1. Summary of electrochemical performances of binder-free CMS/Ni electrode and recently reported binder free electrode materials using three-electrode configurations.

S. No.	Material	Preparation method	Specific capacity (mAh g^{-1})	Specific capacitance (F g^{-1})	Ref
1.	CuS/Ni foam	Hydrothermal	-	1124	[6]
2.	MoS_2/Ni foam	SILAR	-	661	[7]
3.	MoS_2/Mo foil	Hydrothermal	-	192.7	[8]
4.	Ni_3S_2/Ni foam	Hydrothermal	-	1293	[2]
5.	$Co_9S_{8/}$Ni foam	Hydrothermal	-	1775	[9]
6.	NCS/Ni foam	Electrodeposition	-	1712	[10]
7	Co-Mn S/ Ni foam	Electrodeposition	53.4	1000	[11]
8	Ni_3S_2@β-NiS/Ni foam	Solvothermal	-	1158	[12]
9	$ZnCo_2O_4$ /Ni foam	Hydrothermal	-	1620	[13]
10.	Ni-Mo oxide/ Ni foam	Hydrothermal	-	1189	[14]
11.	**CMS/Ni foam**	**Hydrothermal**	**633**	**2278.83**	**This work**

Table S2. Summary of electrochemical performances of CMS/Ni SSC device and recently reported binder-free SSC device.

S. No.	Material	Potential window (V)	Specific capacitance ($F\ g^{-1}$)	Energy density ($Wh\ kg^{-1}$)	Power density ($W\ kg^{-1}$)	Reference
1	$ZnCo_2O_4$/Ni foam	0.8	568	12.5	800	R1[15]
2	Co_3O_4@$CoMoO_4$/Ni foam	0.8	107	10.1	200	R2[16]
3	MoS_2/Carbon cloth	0.8	368	5.42	128	R3[17]
4	MnO_2/ Ni coated porous AAO	0.8	194.23	4.2	151	R4[18]
5	MnO_2/Carbon fiber	1	79	11	529.3	R5[19]
6	$CuCo_2O_4$/Ni foam	1.2	50.75	17	480	R6[20]
7	$Cd(OH)_2$/SS	1.9	51	11.09	799	R7[21]
8	$Co(OH)_2$/GF	1.2	69	13.9	-	R8[22]
9	$Co(OH)_2$/SS	1.2	44	3.96	-	R9[23]
10	**CMS/Ni SSC device**	**0.8**	**265.625**	**23.61**	**1000**	**This work**

***** References R1 to R9 are the references mentioned in the Ragone plot (Figure 4 (F) of the main manuscript.

References:

1 W. Wang, P. Zhang, L. Peng, W. Xie, G. Zhang, Y. Tu and W. Mai, *CrystEngComm*, 2010, **12**, 700–701.

2 K. Krishnamoorthy, G. K. Veerasubramani, S. Radhakrishnan and S. J. Kim, *Chem. Eng. J.*, 2014, **251**, 116–122.

3 V. K. Mariappan, K. Krishnamoorthy, P. Pazhamalai, S. Sahoo and S. J. Kim, *Electrochim. Acta*., 2018, **265**, 514-522

4 K. Krishnamoorthy, P. Pazhamalai, S. Sahoo, J. H. Lim, K. H. Choi and S. J. Kim, *ChemElectroChem*., 2017,**4**, 3302

5 K. Krishnamoorthy, P. Pazhamalai and S. J. Kim, *Electrochim. Acta*, 2017, **227**, 85–94.

6 Y. Zhang, J. Xu, Y. Zheng, X. Hu, Y. Shang and Y. Zhang, *RSC Adv.*, 2016, **6**, 59976–59983.

7 R. N. Bulakhe and J.-J. Shim, *New J. Chem.*, 2017, **41**, 1473–1482.

8 K. Krishnamoorthy, G. K. Veerasubramani, P. Pazhamalai and S. J. Kim, *Electrochim. Acta*, 2016, **190**, 305–312.

9 J. Pu, Z. Wang, K. Wu, N. Yu and E. Sheng, *Phys. Chem. Chem. Phys.*, 2014, **16**, 785–791.

10 S. Sahoo, K. K. Naik, D. J. Late and C. S. Rout, *J. Alloys Compd.*, 2017, **695**, 154–161.

11 S. Sahoo and C. S. Rout, *Electrochim. Acta*, 2016, **220**, 57–66.

12 W. Li, S. Wang, L. Xin, M. Wu and X. Lou, *J. Mater. Chem. A*, 2016, **4**, 7700–7709.

13 B. Guan, D. Guo, L. Hu, G. Zhang, T. Fu, W. Ren, J. Li and Q. Li, *J. Mater. Chem. A*, 2014, **2**, 16116–16123.

14 D. Cheng, Y. Yang, Y. Luo, C. Fang and J. Xiong, *Electrochim. Acta*, 2015, **176**,

1343–1351.

15 S. Wang, J. Pu, Y. Tong, Y. Cheng, Y. Gao and Z. Wang, *J. Mater. Chem. A*, 2014, **2**, 5434–5440.

16 J. Wang, X. Zhang, Q. Wei, H. Lv, Y. Tian, Z. Tong, X. Liu, J. Hao, H. Qu and J. Zhao, *Nano Energy*, 2016, **19**, 222–233.

17 M. S. Javed, S. Dai, M. Wang, D. Guo, L. Chen, X. Wang, C. Hu and Y. Xi, *J. Power Sources*, 2015, **285**, 63–69.

18 A. Kumar, A. Sanger, A. Kumar, Y. Kumar and R. Chandra, *Electrochim. Acta*, 2016, **222**, 1761–1769.

19 Y. Wen, T. Qin, Z. Wang, X. Jiang, S. Peng, J. Zhang, J. Hou, F. Huang, D. He and G. Cao, *J. Alloys Compd.*, 2017, **699**, 126–135.

20 Y. Wang, D. Yang, J. Lian, T. Wei and Y. Sun, *J. Alloys Compd.*, 2018, **741**, 527-531

21 S. Patil, S. Raut, R. Gore and B. Sankapal, *New J. Chem.*, 2015, **39**, 9124–9131.

22 U. M. Patil, S. C. Lee, J. S. Sohn, S. B. Kulkarni, K. V Gurav, J. H. Kim, J. H. Kim, S. Lee and S. C. Jun, *Electrochim. Acta*, 2014, **129**, 334–342.

23 A. D. Jagadale, V. S. Kumbhar, D. S. Dhawale and C. D. Lokhande, *Electrochim. Acta*, 2013, **98**, 32–38.